ELSEVIER

Marine Geology 217 (2005) 283–304

MARINE GEOLOGY
INTERNATIONAL JOURNAL OF MARINE GEOLOGY, GEOCHEMISTRY AND GEOPHYSICS

www.elsevier.com/locate/margeo

Causes of the marine productivity and oxygen changes associated with the Permian–Triassic boundary: A reevaluation with ocean general circulation models

Arne M.E. Winguth[a,*], Ernst Maier-Reimer[b]

[a]*Department of Atmospheric and Oceanic Sciences, 1225 W. Dayton St., Madison, WI 53706, USA*
[b]*Max-Planck-Institute for Meteorology, Bundesstr. 55, 20146 Hamburg, Germany*

Accepted 2 March 2005

Abstract

Widespread anoxic and dysoxic deposition in marine sediments has been associated with a stagnant ocean at the Permian–Triassic (P–Tr) boundary. This P–Tr boundary is also associated with one of the largest mass extinctions of species of the Paleozoic, marking the transition to the Mesozoic. Here we review recent three-dimensional numerical model studies that have investigated possible circulation patterns at the P–Tr boundary. In addition, we conduct new sensitivity experiments with a coupled ocean–atmosphere model of intermediate complexity, including marine chemistry, to study changes of the deep-sea oxygen distribution associated with (1) a significant change in the hydrological cycle and (2) a massive release of methane gas hydrates from marine sediments. Freshening of sea surface water masses by a strong freshwater source along the west coast of south polar Pangea produces a significant local minimum in oxygen in the eastern tropical Panthalassa ocean at intermediate depth and at the sea floor. The methane release experiment with an atmospheric CO_2 concentration of 18 times the preindustrial CO_2 level simulates a strong increase in sea surface temperature (about 4.5 °C) and a vigorous deep-sea circulation. In contrast to the conclusions drawn from previous studies, this reanalysis of the ocean circulation at the P–Tr boundary favors a strong ventilation in most parts of the deep-sea. Thus, a significant change in the oceanic carbon inventories and a reorganization of the marine productivity associated with a stronger biological pump may be required to explain the anoxic sedimentary deposits.

Keywords: mass extinctions; anoxia; paleoceanography; ocean modeling

1. Introduction

The last great transition of the Earth from a cold to a warm climate began around 280 million years ago (Ma), with the final melting of the major southern hemisphere ice sheets of the Late Paleozoic. This

* Corresponding author. Fax: +1 608 262 4874.
E-mail addresses: amwinguth@wisc.edu (A.M.E. Winguth), maier-reimer@dkrz.de (E. Maier-Reimer).

0025-3227/$ - see front matter © 2005 Elsevier B.V. All rights reserved.
doi:10.1016/j.margeo.2005.02.011

marked the onset of warm-climate conditions that lasted ~ 250 million years until the beginning of a cooling trend that culminated in the current Late Cenozoic glacial regime. The circumstances causing the onset of the warm period, the changes within the warm period, and the beginning of the cooling, are the subject of intense current research. Factors being considered include: changes in land/ocean distribution, height and location of mountains, ocean seaways, atmospheric greenhouse gas concentration, terrestrial vegetation, terrestrial/marine biogeochemistry, and the intensity of solar radiation (see Barron and Fawcett, 1995; Crowley, 2000; Crowley and Berner, 2001, for an overview of the role of many of these factors in climate change). The investigation of this long period of geologic time is of great interest to studies of earth system dynamics.

The mass extinction that occurred at the Permian–Triassic (P–Tr) boundary (251 Ma) represented the most extensive species loss of the last 550 million years (Erwin, 1993). Estimates of extinction are about 90% for marine and 70% for terrestrial organisms (Raup and Sepkoski, 1982; Erwin, 1994; Sepkoski, 1995). Several hypotheses have been discussed to explain the complexity of the P–Tr mass extinction. Most hypotheses associate the mass extinction with (1) the long-term reorganization of the carbon cycle, (2) the release of methane stored in methane hydrates, (3) loading of the ocean with toxic gases, (4) large-scale volcanism, or (5) extraterrestrial impacts by asteroids or comets (see Erwin et al., 2002; Berner, 2002, for a review). In this paper we will focus on the following hypotheses associated with mass extinctions.

1.1. Reorganization of the carbon cycle

Broecker and Peacock (1999) suggested that the negative excursion of 2–4‰ in the carbon isotopic composition ($\delta^{13}C$) of marine carbonates and of organic matter at the P–Tr boundary (Fig. 1; Baud et al., 1989; Veizer et al., 1999; Sephton et al., 2002; Payne et al., 2004) may be explained by changes in the global ecosystem induced by the massive mass extinctions. Even higher positive and negative excursions in $\delta^{13}C$ of up to 8‰ have been reported for the Early Triassic over time scales of tens to thousands of years (Payne et al., 2004). The continental ecosystem responsible for the burial of organic matter was disrupted and the relatively efficient marine food web of the Permian changed into a less effective Triassic marine food web. Thus, main burial of organic matter probably moved to the marine environment. The rapid change in ocean chemistry is also evident from a dramatic change in sulfur isotopes (e.g. Holser, 1977; Strauss, 1997, 1999). The secular changes could be related to the redox balance in the sulfur cycle. The observed shift of about 5‰ in the sulfur isotopes ($\delta^{34}S$) from sulfates in evaporites may be explained by a change in the mass of net pyrite formation through bacterial sulfate reduction and burial in the sedimentary reservoir (see Strauss,

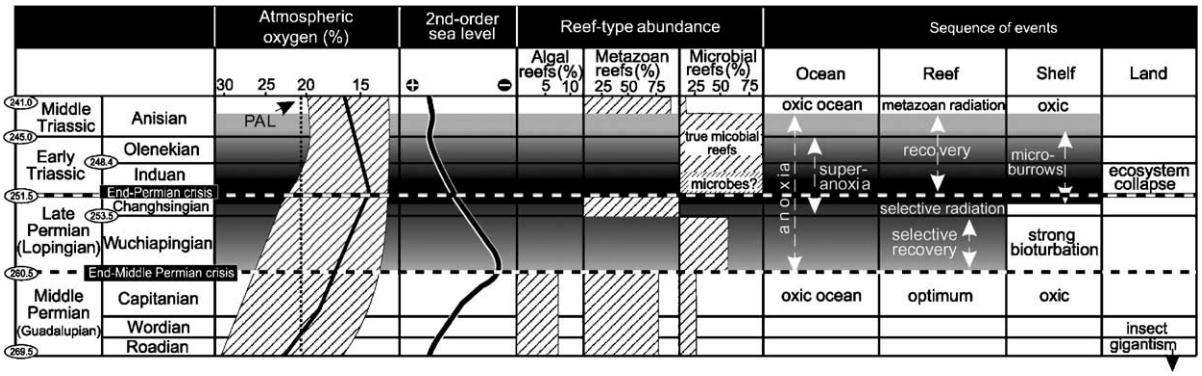

Fig. 1. Composite chart of the Permian–Triassic interval (269.5–241.0 Ma) from Weidlich et al. (2003) including modeled atmospheric oxygen level, second-order sea level reconstruction, and ecosystem collapse and recovery patterns on land and in sea. Darker shading denotes greater intensity of ocean anoxia. PAL is present atmospheric oxygen level (20.9%).

1997, for a review). The greater amount of marine organic matter deposited at the sea floor at the P–Tr boundary is associated with an increase of anoxic bottom waters identified by black, carbon- and sulfide-rich sediments (Isozaki, 1997; Wignall and Twitchett, 2002; Fig. 1). It has been speculated that the anoxia in the Panthalassa oceans were associated with a stagnant or sluggish ocean circulation (Knoll et al., 1996; Ryskin, 2003; Beauchamp and Baud, 2002). Stratified deep-sea water masses, like in the modern Black Sea, are favorable for anoxic conditions.

However, the Neothethyan ocean along the east coast of southern Pangea may have been well-oxygenated by a warm saline deep water formation similar to the Mediterranean Sea (Wignall and Newton, 2003). But saline and warm water would also reduce the solubility of oxygen and would lead to a reduced oxygen concentration in the deep water (solubility ratio between a 0 °C and 24 °C water mass is ~ 1.6). In this paper, we reevaluate the changes in the deep-sea oxygen concentration with several numerical sensitivity experiments.

Table 1
Comparison of Permian ocean simulations obtained from three-dimensional general circulation models

Ocean general circulation model studies	Atmospheric surface forcing	Experiment	Meridional overturning circulation [Sv] (S.H.)	Meridional overturning circulation [Sv] (N.H.)	Max. poleward heat transport [PW] (S.H.)
Otto-Bliesner et al., 2002	Coupled atmosphere–ocean	Present-day	30	30	0.5
	Coupled atmosphere–ocean	Cretaceous	70	30	1.8
Smith, 2004	Coupled atmosphere–ocean	Pangea World	101	93	1.28
Kutzbach et al., 1990[a]	Prescribed forcing from Kutzbach and Gallimore (1989)	Experiment I	20	20	1.7
Hotinski et al., 2001	Prescribed zonal mean forcing from Rees et al. (1999)	High Gradient	> 80	15	N/A
	Paleocene–Eocene boundary (Zachos et al., 1994; Bice et al., 2000)	Low Gradient	20	15	N/A
Zhang et al., 2001	Prescribed wind stress and temperature and fresh water fluxes (after Kutzbach and Gallimore, 1989)	Thermal Mode	40	N/A	1.8
	Same as thermal mode but with increased freshwater fluxes	Haline Mode	14[b]	14[b]	0.4
Winguth et al., 2002, and this study	Freshwater fluxes and momentum fluxes (Gibbs et al., 2002) Heat fluxes by EBM	$1 \times CO_2$	60	N/A	2.4
		$2 \times CO_2$	60	25	1.7
		$4 \times CO_2$	55	30	1.7
		$8 \times CO_2$	55	30	1.8
	With additional S.H. freshwater input	$4 \times CO_2$WFL	20	55	1.5
		$8 \times CO_2$WFL	25	55	1.5
	Methane release[c]	$18 \times CO_2$	65	55	1.7
Poussard et al., 1999	Coupled atmospheric energy balance ocean general circulation model	10x_wfcs.1 Ordovician	36	26	2.1

None of the model studies produced a stable stagnant ocean circulation. Strongest reduction is found in the haline mode (Zhang et al., 2001), which is prone to instability. Other model simulations for a superocean (e.g. for the Ordivician, Poussard et al., 1999; for the Cretaceaous, Otto-Bliesner et al., 2002; and for an idealized Pangean continental configuration, Smith, 2004) confirm the results of a vigorous thermohaline circulation.

[a] Kutzbach et al. (1990) used a symmetric idealized continental configuration.

[b] The haline mode induces sinking in subtropics and a stagnant deep sea.

[c] For methane release values are shown after 2000 yr of integration.

1.2. Voluminous release of methane from marine and permafrost clathrates

A massive methane release could have been triggered by a marine regression as suggested by Erwin (1993). A revised analysis of Erwin et al. (2002) questions the regression hypothesis due to growing evidence for marine transgression. Krull and Retallack (2000) suggested that a drop in sea level (Fig. 1) in an initial phase destabilized clathrates while the Siberian traps further intensified the greenhouse warming. Ryskin (2003) proposed that dissolved methane could have been accumulated in oceanic water masses prone to stagnation. Consequences of a massive release of methane from marine sediments and permafrost into the ocean and atmosphere have been discussed in several publications (e.g. Erwin, 1993; Krull and Retallack, 2000; Berner, 2002; Heydari and Hassanzadeh, 2003; Ryskin, 2003; Retallack et al., 2003). Aerobic dissociation of methane in the ocean would lead to a strong increase of CO_2, a significant decrease in the dissolved oxygen in the water column, and favor high concentrations of Ca^{2+} and HCO^{3-}. Radiative forcing of methane in the atmosphere depends on the methane concentration (methane has an about 20 times higher global warming potential than CO_2) and a post-apocalyptic greenhouse created by the release of methane may have triggered a widespread event of vertebrate mortality (Retallack et al., 2003). However, the residence time of methane in the atmosphere is low (~ 10 yr) and may result only in a small rise in atmospheric CO_2 concentration in the long term. Here, we will investigate the response of the ocean circulation and oxygen distribution in response to a massive greenhouse perturbation.

In this paper, we will review how changes in the ocean circulation influence the reorganization of the carbon cycle and how the ocean circulation and oxygen distribution may be altered by the release of massive methane into the atmosphere–ocean system. It is not the purpose of this paper to evaluate all other important hypotheses on mass extinctions, but results from our work could be important for some aspects of the other hypotheses. We will reexamine studies with three-dimensional ocean general circulation models listed in Table 1 with respect to geographic, thermal, and hydrological boundary conditions and the resulting circulation patterns for the Late Permian (Section 2). In addition, we designed new experiments with a coupled ocean–atmosphere model of intermediate complexity to investigate the response of the Permian thermohaline circulation to a freshwater perturbation and to a gas hydrate release. Section 3 describes changes of marine productivity and deep-sea oxygen distribution in response to changes in the circulation pattern from the different models and experiments. The possibility of a stagnant ocean and associated anoxia will be explored by the intercomparison of the most recent three-dimensional modeling studies of Hotinski et al. (2001), Zhang et al. (2001), Winguth et al. (2002), and the new experiments described above. The model results are compared with water mass reconstructions from climate-sensitive sediments, and an overall summary and conclusion are given in Section 4.

2. Permian ocean model studies

2.1. Geographic boundary conditions: topography and land–sea distribution

The paleogeographic basemaps for the modeling studies of Zhang et al. (2001), Hotinski et al. (2001), and Winguth et al. (2002), including land–sea distribution, bathymetry and land surface elevation, were taken from the Paleogeographic Atlas Project of the University of Chicago (Fig. 2, Ziegler et al., 1997; http://www.pgap.uchicago.edu). Continental positioning is a crucial boundary condition for the atmospheric and oceanic circulation. The ocean circulation also depends on the mean depth of the ocean (Bice, 1997) and on the bathymetry. All modeling studies assumed a flat bottom bathymetry, since the positions of mid-ocean ridges are not known for the Permian circulation (Ziegler, personal communication). The maximum depth was set to 4000 m (Zhang et al., 2001; Winguth et al., 2002) based on the mean depth of the modern ocean. In the case of the study of Hotinski et al. (2001), a flat bottom was assumed at 5150 m depth. A smoothed transition from the continental shelves to the deep ocean is derived from the modern bathymetry (Fig. 2). The deep Tethys is cut off from the Panthalassa Ocean. The assumption of a flat bottom is highly simplified, and a Permian

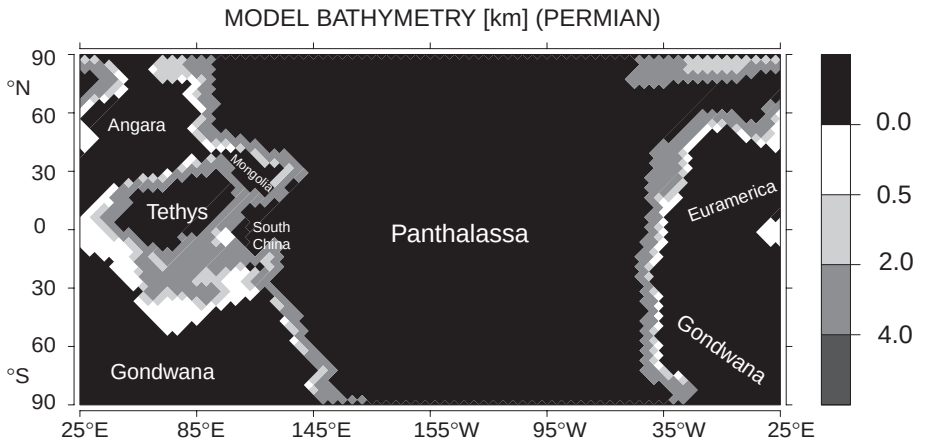

Fig. 2. Model bathymetry for the Late Permian (from Winguth et al., 2002).

bathymetry with mid-ocean ridges may alter the results of the modeling studies.

The Permian continental configuration is well known, except for the position of islands in the Tethys Sea which belong nowadays to Southeast Asia. Rees et al. (1999, 2002) discussed the uncertainties of the positions of land masses for these regions. The altitude of Pangea mountain chains has a relevant impact on the climate simulations (Otto-Bliesner, 1993, 1998; Fluteau et al., 2001) and has been specified for the atmospheric model simulations (Gibbs et al., 2002). The estimates of the orography are based on literature on geochronology, tectonics, sedimentary provinces, paleovolcanism, and paleogeology.

Because of the coarse-resolution model grid, continents in Hotinski et al. (2001) and Winguth et al. (2002) were extended to the pole. A more moderate climate is generated if high latitude land is removed from the southern continent so that warm ocean currents can penetrate into the polar regions of Gondwana. For the new experiments discussed below we decided to use the Wordian (265 Ma) topography, because (1) model results would be directly comparable with the Winguth et al., 2002 simulation, (2) major changes in the land-sea distribution from the Wordian to the Changhsingian (251 Ma) at the Permian–Triassic are generally not resolved by a coarse resolution model, and (3) effects of topographic changes such as open seaways in the polar regions have already been explored in, e.g. Winguth et al. (2002). The latter study explored the sensitivity of the circulation to an open seaway in the northern and southern hemisphere by removing the land between 70° and 90° northern (N) and southern (S) latitude.

2.2. Ocean circulation

2.2.1. Sensitivity of the circulation to formulation of thermal and haline boundary conditions

In this section we will review possible Late Permian circulation patterns in response to different formulations of the forcing boundary conditions. An overview is found in Table 1.

Following the approach of Kutzbach et al. (1990), Hotinski et al. (2001) applied prescribed boundary conditions of temperature, salinity, and wind stress from an atmospheric climate scenario (Rees et al., 1999) to force the Modular Ocean Model (MOM). In a first scenario, the ocean model simulates a high meridional pole to equator sea surface temperature gradient (~ 35 °C in the southern hemisphere and ~ 28 °C in the northern hemisphere), producing a vigorous asymmetric thermohaline circulation with a maximum strength of about 80 Sv (1 Sv = 10^6 m^3 s^{-1}) for the southern hemisphere cell (Table 1). The strength of the overturning circulation is about 4 times higher than in the simulation of Kutzbach et al. (1990) and more consistent to a recent coupled atmosphere–ocean circulation of study of Smith (2004) with an idealized continental configuration as a result of a much stronger equator-to-pole density gradient. In a second,

low-gradient scenario with a weak equator-to-pole temperature difference (12–18 °C) the reduced density gradient produces a circulation of 20 Sv, which is comparable to water masses formed in the modern North Atlantic and to results from Kutzbach et al. (1990). The low-gradient scenario is in better agreement to the paleoclimatic evidence indicating a moderate climate over Gondwana at the end of the Permian (see Rees et al., 2002). However, the use of a prescribed zonal mean atmospheric forcing for the ocean circulation in Hotinski et al. (2001) may be a too simplified approach for a description of the Permian climate neglecting important atmospheric–oceanic feedback processes.

Two circulation scenarios were discussed in the study of Zhang et al. (2001) using the MIT ocean model: The first scenario is based on the study of Kutzbach and Gallimore (1989) with a weak surface wind stress, a weak pole-to-equator temperature gradient, and a freshwater flux (evaporation–precipitation) comparable to the modern value. In the thermal mode, a strong vertical overturn in the southern high latitudes forms a vigorous highly asymmetric circulation, too, with a maximum transport of 40 Sv (Table 1). Large southward heat transports are in the order of 1.8 PW with about 6 °C difference between the warm South Pole and a cold North Pole. A second class of scenarios (haline mode circulation) used the same zonally averaged prescribed boundary conditions of wind stress and temperature as the first scenario, but different amplitudes in freshwater fluxes. Increasing the amplitude of the freshwater fluxes by a factor of 2 yielded a reduced overturning circulation (~ 14 Sv) with warm intermediate water formed in the tropics, and a more symmetric poleward heat transport (0.4 PW towards the South Pole). In this quasi-stationary scenario a stagnant ocean is reproduced. In contrast to the first solution, the haline mode is sensitive to perturbations in the forcing boundary conditions and prone to instability (Marotzke, 1989). The high sensitivity of the thermohaline circulation against perturbations may also be a result of the formulation of the mixed boundary conditions (prescribed temperature and flux formulation for freshwater) (Mikolajewicz and Maier-Reimer, 1994).

Winguth et al. (2002) used a coupled ocean–atmosphere model of intermediate complexity, the coupled atmospheric energy balance model and large-scale geostrophic ocean general circulation model (LSG/EBM), to study the response of the Permian ocean circulation to various atmospheric CO_2 concentrations (a description of the model is given in Appendix A). For $1\times CO_2$ (preindustrial atmospheric CO_2 concentration), large sea ice coverage in the northern hemisphere prevents deep water formation and a strong heat exchange with the atmosphere in the northern high latitudes yields a thermohaline circulation dominated by a southern circulation cell of 80 Sv, consistent with predictions of Zhang et al. (2001) and Hotinski et al. (2001). Experiments with increased CO_2 levels produce decreased northern sea ice coverage (and reduced meridional density gradients), increased formation of deep water in the northern high latitudes, increased sea-to-air heat exchange in polar regions, and a strengthened northern meridional circulation cell (~ 30 Sv for $8\times CO_2$). However, even with the $8\times CO_2$ levels the southern circulation cell with 60 Sv is dominant, which must be a consequence of the asymmetrical land–sea distribution (a symmetrical cell can be obtained if symmetrical continent configuration and surface buoyancy forcing are applied; Kutzbach et al., 1990). In this study, we performed additional sensitivity experiments to investigate the response of the thermohaline circulation to a southern hemisphere freshwater source of 2 Sv in southwest Gondwana. The magnitude and location of the hypothetical freshening of the surface is somewhat arbitrary and designed to be an extreme test of regional changes in the boundary conditions, since feedback processes associated with the hydrological cycle are not considered in the model. The freshening in the south polar sea surface results in an increase in stratification of southern hemisphere water masses relative to the $4\times CO_2$ baseline experiment of Winguth et al. (2002). Because of the stratification, pole-to-equator surface air temperature gradients in the southern hemisphere are doubled over the Panthalassa (increase of 20 °C) and surface temperatures over the interior of Gondwana lowered by about 10 °C (Fig. 3c). The vertical overturning is reduced by 64% relative to the $4\times CO_2$ baseline experiment (Fig. 3a). Interestingly, the northern hemisphere circulation cell (Fig. 3g) is more vigorously ventilated relative to the $4\times CO_2$ baseline experiment (Fig. 3e) as a result of the changes in the pole-to-pole surface density gradients.

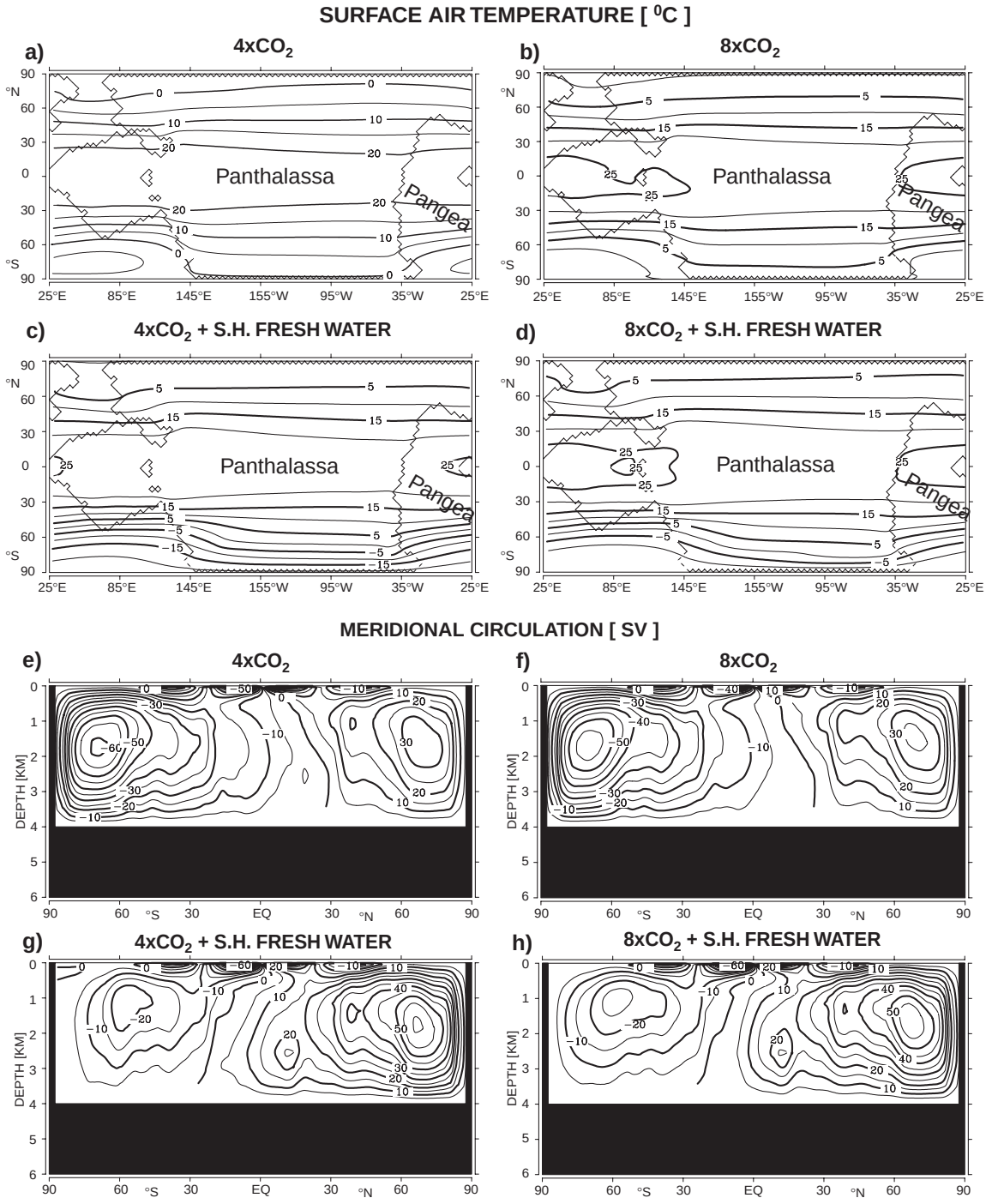

Fig. 3. Top: Annual average of modeled surface air temperature (in °C) for the Late Permian climate for (a) $4\times CO_2$, (b) $8\times CO_2$, (c) $4\times CO_2$ with freshwater input in the southeastern Panthalassa and (d) $8\times CO_2$ with freshwater input in the southeastern Panthalassa (contour interval 5 °C). Bottom: Zonally averaged meridional circulation with (e) $4\times CO_2$, (f) $8\times CO_2$, (g) $4\times CO_2$ with freshwater input in the southeastern Panthalassa and (h) $8\times CO_2$ with freshwater input in the southeastern Panthalassa (contour interval: 5 Sv=5×10^6 m^3 s^{-1}).

The plot of the $8\times CO_2$ experiment with a freshwater source in the southern hemisphere (Fig. 3d) shows a 5 °C increase in the Gondwana surface temperature related to the change in the radiative forcing and a 20% increase in the overturning circulation relative to the $4\times CO_2$ freshwater experiment (note that the freshwater forcing differs in the $8\times CO_2$ experiment, Fig. 3f; see Winguth et al., 2002, for details). The meridional circulation in the southern hemisphere is weakened by 30 Sv in the $8\times CO_2$ freshwater experiment (Fig. 3h) relative to the $8\times CO_2$ experiment (Fig. 3f) as a result of an increased stratification, while the northern hemisphere circulation cell is about 20 Sv stronger.

2.2.2. Sensitivity of the circulation to a massive methane release

Here, we performed a sensitivity experiment with the coupled LSG/EBM to test the response of the ocean's thermal structure and circulation to a massive methane release. The sudden methane release with $\delta^{13}C=-65‰$ may be capable of reproducing a maximum measured short-term drop in the oceanic value of $\delta^{13}C$ by up to 8‰ at the Permian–Triassic boundary (Baud et al., 1989; Bowring et al., 1998). However, the total integrated mass of released methane needed is about 4200 Gt C (1 Gt $C=10^{12}$ kg C) (Berner, 2002). Much higher drops in $\delta^{13}C$ (up to 10‰) would require about twice as much methane (Krull and Retallack, 2000; Twitchett et al., 2001, Payne et al., 2004). Ryskin (2003) proposed that an amount of about 7500 Gt C was released quasi-instantaneously (within weeks perhaps) at the Permian–Triassic boundary, and that would have led to an equivalent $18\times CO_2$ concentration ($4\times CO_2$ baseline level plus $14\times CO_2$ by methane release) with a radiative forcing of 18.2 W m^{-2} (see Eq. (1); Appendix A.1). However, the amount of the methane gas release is highly speculative. Here we test the response of the ocean circulation to a single CO_2 perturbation by assuming that methane has a relatively short lifetime of about 10 yr and is immediately converted into atmospheric CO_2 (which is similar to the approach of Berner, 2002). However, the radiative forcing of methane even with a relatively short lifetime is significantly higher than that of CO_2 and thus the simulation presented here is likely to underestimate the radiative perturbation. Two CO_2 perturbation scenarios with the amount of carbon released of 7500 Gt C and 4200 Gt C (Fig. 4a) investigate the response of the ocean circulation to a massive carbon release. The prescribed exponential decline of the atmospheric CO_2 concentration is adapted from modern CO_2 perturbation experiments by Maier-Reimer et al. (1996) and does not consider changes in the geosphere (such as weathering). With the CO_2 perturbation in radiative forcing described here (Fig. 4a), mean temperature at the sea surface increases by about 3.5 °C and 2.5 °C, respectively, after 100 yr of integration (Fig. 4b) and in the deep-sea by about 2 °C and 1.1 °C, respectively, after 700 yr of integration (Fig. 4c).

In addition, an $18\times CO_2$ experiment ($4\times CO_2$ baseline experiment plus $14\times CO_2$ by continuous methane release) with no exponential decline was conducted to be more consistent with a long-term isotopic shift over several thousand years measured in the sedimentary record. After 2000 yr of integration, the sea surface temperature exceeds 32 °C in the Tethys Sea, which is well ventilated. Mean surface temperatures are 4.5 °C higher than the $4\times CO_2$ baseline experiment. The equator-to-pole temperature gradient in the south Panthalassa is about half compared to the modern South Pacific gradient (Fig. 5a). A vigorous polar deep water formation and a strong poleward heat transport produce a well-ventilated warm deep-sea (about 4.5 °C warmer than in the $4\times CO_2$ baseline experiment) and a strong thermohaline circulation (Fig. 5b).

2.3. Export production and oxygen

In this section, we will summarize the response of export production and oxygen to changes in the ocean circulation. We added a simplified biogeochemical model (Winguth et al., 1999; Appendix A.2) to the LSG/EBM to predict oxygen concentration for the Panthalassa ocean.

2.3.1. Sensitivity of oxygen distribution to changes in thermal and haline boundary conditions

In the high-gradient case of Hotinski et al. (2001), most of the water masses are characterized by high oxygen values except for intermediate waters of the western coast of Pangea. In the reduced-gradient case, the simulated sluggish circulation favors low to

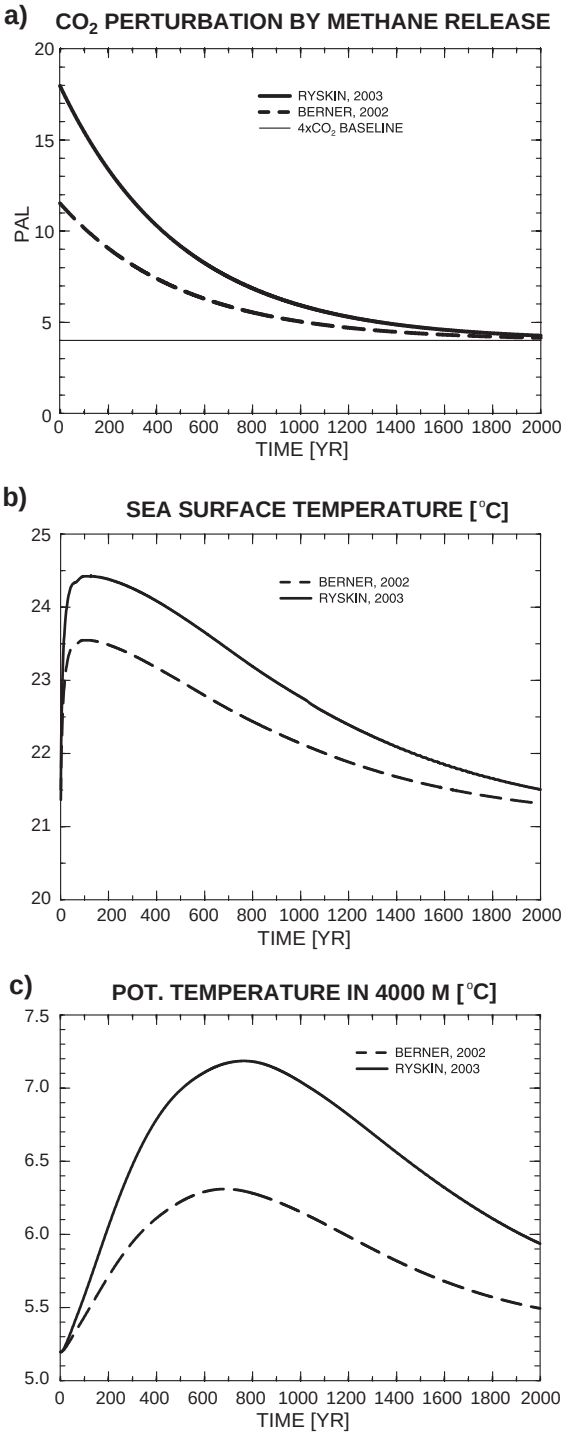

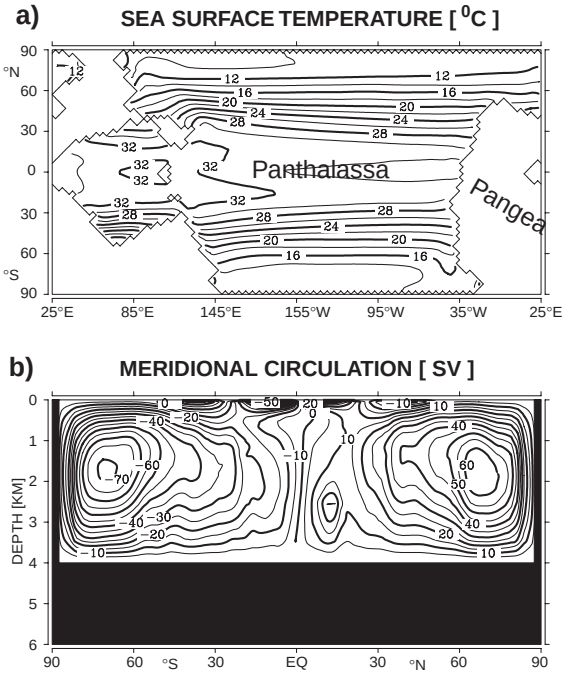

Fig. 5. (a) Annual-average of modeled sea surface temperature (in °C; contour interval 2 °C) and (b) zonally averaged meridional circulation (contour interval: 5 Sv) in response to a 18×CO_2 experiment as a result of a 7500 Gt C methane release over several thousand years (shown are values after 2000 yr of model integration).

negative oxygen concentrations in the deep-sea with values below 50 μmol L^{-1} in the northern hemisphere (see Fig. 3 in Hotinski et al., 2001). It is interesting to note that earlier studies have argued that anoxic conditions may also have been associated with a strong thermohaline overturning circulation. As proposed by Berger (1978) and Saltzman and Barron (1982), saline bottom water produced in the subtropics by evaporative processes may not have been associated with a stagnant ocean. The warm bottom water would have reduced significantly the solubility

Fig. 4. (a) CO_2 perturbation relative to the preindustrial CO_2 concentration (PAL) as a result of a massive methane release from marine sediment. Perturbations are taken according to Ryskin (2003; solid) and Berner (2002; dashed). Here it is assumed that the methane is directly oxidized to CO_2 in either case (see text). Time constant of 350 yr is assumed for the decline of atmospheric CO_2 (similar to Fig. 1 in Maier-Reimer et al., 1996). Increase in global average surface temperature (b) and deep-sea temperature at 4000 m depth (c) as a result of the CO_2 perturbations.

of oxygen and oxygen concentration, which could have promoted anoxic sedimentation. Another proposal by Sarmiento et al. (1988) states that the anoxic conditions are related to the strength of the thermohaline circulation overturning, because primary production is controlled by the nutrient supply in the euphotic zone and thus related to the upwelling of nutrients from layers below the euphotic zone. A reduction in oxygen may therefore be brought about by an increased export production associated with an increased upwelling or vertical overturning. The use of a box model, as applied in the study of Sarmiento et al. (1988), may, however, significantly underestimate the new production, as documented in Archer et al. (2000a), because the lack of resolution inhibits shallow water redissolution of sinking nutrients.

Consistent to the high-gradient case of Hotinski et al. (2001), the well-mixed circulation for the thermal mode of Zhang et al. (2001) produces an oxygen minimum for intermediate waters and a high oxygen concentration of over 200 μmol L^{-1} for the deep-sea. In contrast, lowest values of dissolved oxygen (concentrations below 20 μmol L^{-1}) are simulated in the haline mode with sluggish deep-sea circulation favoring the accumulation of carbon in the near bottom layers. However, the use of negative oxygen concentrations in the study of Hotinski et al. (2001) may be problematic since the negative concentration can be transported by diffusion and/or advection into well-ventilated regions where it artificially reduces the oxygen values.

We used the same experiment setup as discussed in Section 2.2 to predict changes in oxygen with the LSG/EBM including the marine carbon cycle. Export production for the 4×CO_2 baseline experiment (Fig. 6a) is pronounced in the eastern Panthalassa and east of South China. These features are associated with Ekman-induced upwelling of nutrient waters from the subsurface. Oxygen distribution in the 4×CO_2 experiment (Fig. 6b) shows a strong minimum around 1000 m depth in the eastern equatorial Panthalassa, about 200 m deeper than in the thermal mode of Zhang et al. (2001) or in the high-gradient simulation of Hotinski et al. (2001). The deep-sea is generally well ventilated with highest oxygen concentrations in the western part of Panthalassa and lowest concentrations above zones of maximal productivity (Fig. 7a). Differences

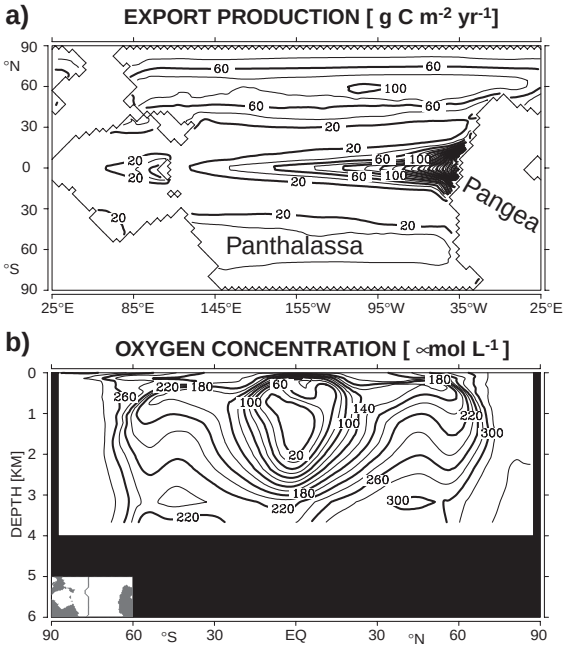

Fig. 6. (a) Annual-average of modeled export production (in g carbon m^{-2} yr^{-1}) and (b) N–S cross section of modeled dissolved oxygen in μmol L^{-1} of the Panthalassa for the Late Permian climate with 4×CO_2 (contour interval 10 g C m^{-2} yr^{-1}; 20 μmol L^{-1}).

between the 8×CO_2 simulation and the 4×CO_2 baseline simulation are relatively small (Fig. 7b). This is because poleward heat transport and strength of the deep-sea circulation in the two experiments are comparable.

The 4×CO_2 simulation with freshwater input predicts a higher accumulation of organic carbon in the deep-sea (Fig. 7c) in response to a reduced circulation in the southern hemisphere. In the 8×CO_2 experiment, the reduced ventilation of the southern hemisphere affects the oxygen concentration in the tropical region, where a wide low-oxygen region is formed in the center of the basin (Fig. 7d). Consistent with the low-gradient simulation of Hotinski et al. (2001) and the haline mode of Zhang et al. (2001), this simulation indicates that a more sluggish circulation may lead to extended anoxic conditions in the deep-sea. However, our predicted oxygen concentrations are significantly higher in comparison to the other studies, because of a strong northern hemisphere circulation cell in the freshwater input experiments.

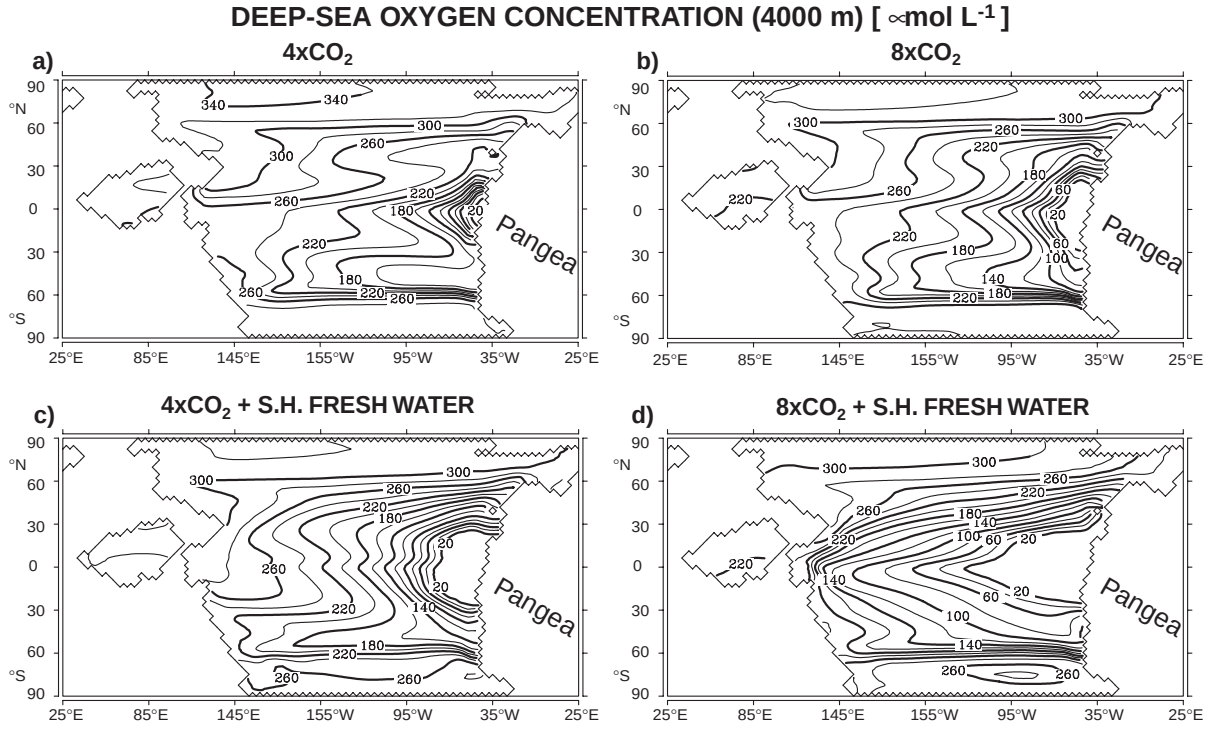

Fig. 7. Annual average of modeled dissolved oxygen (in μmol L^{-1}) in 4000 m depth for the Late Permian climate with $4\times CO_2$ (a), $8\times CO_2$ (b), $4\times CO_2$ and southern hemisphere freshwater input (c), $8\times CO_2$ and southern hemisphere freshwater input (d) (contour interval 20 μmol L^{-1}).

2.3.2. Sensitivity of oxygen distribution to a reduced biological pump

Here we follow the idea of a less efficient food web associated with the Permian–Triassic boundary (Broecker and Peacock, 1999). Guided by the reconstructions of extinction levels at the P–Tr boundary (see, e.g. Sepkoski, 1995; Knoll et al., 1996), we reduced the export production to 10% (Eq. (2), Appendix A.2) of its reference level used for the Permian $4\times CO_2$ simulation. The strong reduction in the production yields a reduction of the vertical transport of carbon in the deep-sea and hence a reduction of the material to be mineralized in the bottom layers (Fig. 8a). This decrease in the decomposition of organic material results in an increase of the oxygen content in the deep-sea. Even the eastern tropical Panthalassa, with the highest export production, is characterized by a high deep-sea oxygen concentration of 220 μmol L^{-1} (Fig. 8b).

2.3.3. Sensitivity of oxygen distribution to a massive methane release

The effective circulation associated with the greenhouse warming by the methane perturbation produces high oxygen concentrations in the high-latitude deep-sea. The highest oxygen concentration of over 280 μmol L^{-1} is found in the deep northeastern Panthalassa (Fig. 9). Lateral plots of 4000 m depth indicate a strong east–west gradient of 200 μmol L^{-1} for the tropical deep-sea. Low oxygen concentrations (< 20 μmol L^{-1}) are simulated only in the eastern part of the superocean for the intermediate depth (~ 1000 m) and in the bottom layers. Here, we make the simplified assumption that the methane from marine sediments is immediately released to the atmosphere, so that no methane is oxidized. This assumption is based on the paleoclimatic evidence from the Paleocene/Eocene boundary (Dickens, 2003), indicating that the stable carbonate isotopic signature from a possible gas hydrate release can first

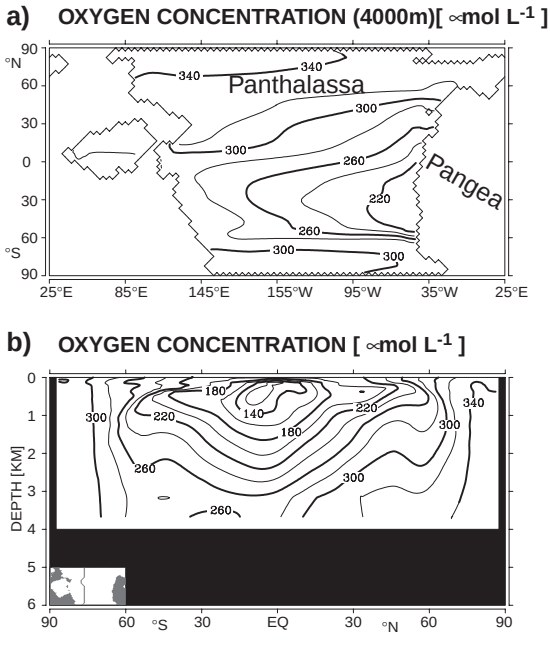

Fig. 8. (a) Annual average of modeled dissolved oxygen (in μmol L^{-1}) in 4000 m depth, and (b) N–S cross section of modeled dissolved oxygen in μmol L^{-1} for the Late Permian climate with $4\times CO_2$ and reduced biological production (10% of its reference value; see text) (contour interval 20 μmol L^{-1}).

be seen in surface foraminifera shells. Our simulations did not consider long-term changes in the atmospheric oxygen content (Fig. 1), possibly as low as 15% at the P–Tr boundary (as simulated by Berner, 1999, 2001). Alternative oxygen estimates involving buffering feedbacks indicate a less pronounced change in the oxygen content (Lenton, 2001). The change of the oxygen concentration by a methane release is probably only secondary for the entire oxygen budget calculation.

3. Comparison of model results with climate-sensitive sediments

Ziegler et al. (1998) constructed a climate map for the Late Permian (Changhsingian, Fig. 10a) based upon sediment distribution and the present-day relationship of sediments to characteristic water masses. The climate-sensitive sediments have been associated with modern marine climate properties, in particular temperature, salinity and productivity-related effects. The water mass boundaries are listed in Ziegler et al. (1998) and Winguth et al. (2002). The water masses of Ziegler et al. (1998) (Fig. 10a) are classified in eight categories and are compared with the Permian baseline experiment $4\times CO_2$ (Fig. 10b), the $8\times CO_2$ experiment with southern hemisphere freshwater input (Fig. 10c), and the methane release experiment (Fig. 10d).

3.1. Glacial climate

3.1.1. Data

Occurrence of permanent ice flows generated by outflow of cold air. Sediments, like tills along coasts, are known in the Early Permian but have not been found in Late Permian rocks.

3.1.2. Model

In the ocean, sea ice cover (sea surface temperatures <-1.8 °C) is not simulated in all experiments with CO_2 levels above $2\times CO_2$.

3.2. Cold temperate climate

3.2.1. Data

The water masses are defined by the extent of sea ice in the winter season and correspond closely to the 0 °C isotherm. Dropstones and rhythmites would be indicative of this environment in the fossil record but have been not identified for the Changhsingian in the reconstructions.

3.2.2. Model

The model with $4\times CO_2$ and higher (Fig. 10b and d) simulates moderate conditions along the south polar east coast from Gondwana in agreement with the data. In the $4\times CO_2$ experiment with freshwater input (not shown), a cold temperate region ranges from the South Pole to 60°S on the east coast of Gondwana. The prediction from this simulation would be in better agreement with Capitanian or Wordian deposits.

3.3. Wet temperate climate

3.3.1. Data

Temperatures between 0 °C and 20 °C and brackish conditions (salinity below 32) define this climate zone. Peats develop around the margins of

these characteristic water masses and organic muds are commonly found in the center of these areas with high precipitation. The associated surface runoff provides for abundant nutrients and a stratified water column, which in turn allows for organic preservation. The geological data (Fig. 10a) for this water mass are best seen around Angara but also occur around the southern Tethys Sea shoreline (northern India).

3.3.2. Model

Simulated high precipitation (Gibbs et al., 2002) and low salinities of the high-latitude west coasts of Angara and along the shore of the southern Tethys Sea agree with the geological recognition of the wet temperate climate category. Simulations with freshwater input in the southern hemisphere (Fig. 10c) are characterized by brackish conditions along the coasts of Gondwana (up to about 40°S at the east coast). These brackish conditions result from the advection of freshwater from its high-latitude source at the west coast. The wet temperate climate zone has not been identified from sedimentary deposits for the Changhsingian (Fig. 10a), but for the Arktinskian after the Early Permian deglaciation (Ziegler et al., 1998).

3.4. Temperate climate

3.4.1. Data

Temperature in this climate zone ranges between 0 °C and 20 °C and salinity between 32 and 37. No particular climate indicators have been identified for this zone, but peats are quite common due to low evaporation rates in mid- to high latitudes.

3.4.2. Model

The equatorial margin of the water mass in this climate zone is placed around 30° latitude for the 4× CO_2 simulation (Fig. 10b), similar to the reconstructed equatorial margin from climate-sensitive sediments (Fig. 10a). The bias between model results and the reconstructions on the west coast of Pangea can be explained by the more poleward location of main upwelling areas, which are centered around the equator in the model as a response to the wind stress and bathymetry. Experiments with CO_2 concentrations greater than 4×CO_2 are characterized by a more poleward 20 °C isotherm (located around 50° latitude; Fig. 10d). Such a shift has been suggested from the Permian conodont provincialism for the Wuchiapingian warming (Mei and Henderson, 2001).

3.5. Cool subtropical upwelling zones

3.5.1. Data

This category is defined by zones which are mainly limited to the subtropical belt and the equatorial region where Ekman-induced upwelling produces high organic productivity and nutrient content. Formation of organic muds and phosphorites constitutes the recognition of these upwelling zones. No attempt was made to map the equatorial upwelling zone as the Permian ocean floor has been subducted and the sedimentary evidence destroyed.

3.5.2. Model

Upwelling is defined to have upward current velocities greater than 1×10^{-6} m s^{-1} (Fig. 10b–d). Typical regions are the coastal upwelling zones along the west coast of Gondwana. A strong upwelling belt is located along the equator, similar to the modern Pacific and around islands.

3.6. Dry subtropical climate

3.6.1. Data

Areas with low precipitation-minus-evaporation with salinity greater than 37 provide favorable conditions for evaporite deposition in coastal lagoons and broad platform seaways (Fig. 10a).

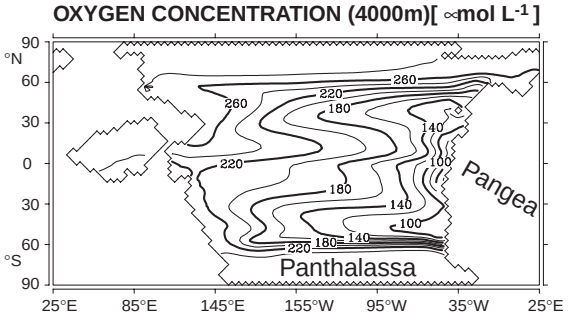

Fig. 9. Annual average of modeled dissolved oxygen (in μmol L^{-1}) in 4000 m depth from the 18×CO_2 experiment (shown are values after 2000 yr of model integration; contour interval 20 μmol L^{-1}).

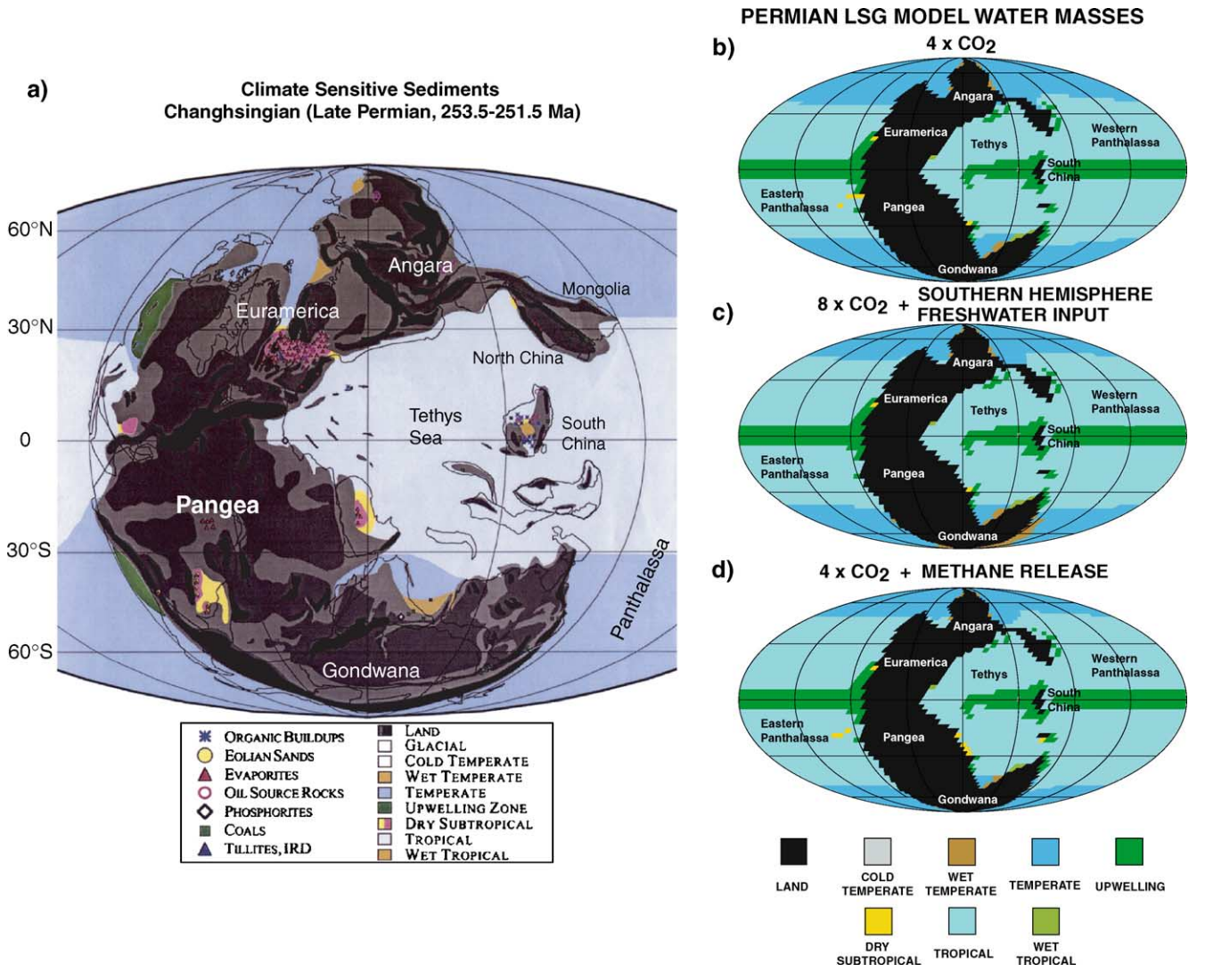

Fig. 10. (a) Changhsingian (Late Tatarian, Late Ochoan) climate-sensitive sediments and reconstructed water masses from Ziegler et al. (1998). Water mass classification derived from the climate simulation with $4\times CO_2$ (b), $8\times CO_2$ with freshwater input in the southern hemisphere (c), and methane release experiment equivalent to $18\times CO_2$ concentration (d) using the classification scheme of Table 2 in Winguth et al. (2002).

3.6.2. Model

Low precipitation and high salinities are simulated along the southeastern Tethys Sea, South China, and the west coast of Euramerica in agreement with the geological evidence. In addition, embayments along the northern coast of Euramerica have been identified as dry from model simulations (Gibbs et al., 2002) and geological data. However, our ocean model does not resolve this area because of its coarse resolution (Fig. 10b–d). Overall, the simulations agree reasonably well with the sedimentary deposits.

3.7. Tropical climate

3.7.1. Data

Surface temperatures greater than 20 °C and normal salinity, which allows carbonate build-up and bottom productivity, characterize this water mass (Fig. 10a). Carbonate build-ups are generally not found in the geological past above 35° of latitude, as shown by paleomagnetic data (Hulver et al., 1997). This latitudinal restriction constitutes the zone of light penetration to the sea floor as controlled by the sun's zenith angle (Ziegler et al., 1984).

3.7.2. Model

The $4\times CO_2$ model simulation (Fig. 10b) is in agreement with the climatic reconstructions (Fig. 10a), but differences on the west coast of Pangea are associated with upwelling areas, which cannot be entirely resolved with the coarse model resolution. As discussed in Section 3.4, tropical climate zones are extended more poleward in climate simulations with a higher radiative forcing than $4\times CO_2$.

3.8. Wet tropical

3.8.1. Data

Wet tropical areas are defined to have sea surface temperatures above 20 °C and relatively brackish conditions (salinities below 32). Organic-rich shales do not seem to be associated with wet tropical climate at modern times, but they almost certainly occurred in the Wordian (e.g. in the South China, Fig. 10a).

3.8.2. Model

Wet tropical conditions are simulated in the southern Tethys Sea (Fig. 10b–d) in the $4\times CO_2$ circulation. This area is characterized by high river runoff, and/or high precipitation (e.g. along the intertropical convergence zone) and correlates well with tropical coals in the sedimentary record.

4. Summary and conclusions

We reevaluated several model studies (Table 1) predicting the deep-sea circulation of the Panthalassa with various equator-to-pole density gradients. In addition, we have tested the sensitivity of a coupled ocean–atmosphere model with intermediate complexity in response to a strong freshwater perturbation in the southern hemisphere and to a massive methane release into the atmosphere. A southern hemisphere freshwater input reduces the strength of the overturning circulation and produces low oxygen concentrations in the tropical eastern Panthalassa, while the massive methane release produces a strong circulation and a well-ventilated deep-sea with oxygen-rich water masses. In summary, most of the model simulations, in particular those with a more complex coupling of the atmosphere–ocean circulation, predict a vigorous deep-sea circulation for the Permian Panthalassa ocean with relatively high oxygen concentrations.

Support for a well-ventilated deep-sea in the superocean comes from model studies with different geography. For example, an Ordivician climate simulation (Poussard et al., 1999) and a fully coupled atmosphere–ocean simulation for the Cretaceaous (Otto-Bliesner et al., 2002) have also produced a vigorous ventilation. We emphasize, however, that these findings may strongly be influenced by the inevitable assumption of a flat bottom; hydrographic profiles, for instance, clearly demonstrate in the modern ocean how ridges block the ventilation.

Comparison of the model simulations with water mass reconstruction from climate-sensitive sediments indicates a general agreement between the predictions and geological findings. Poleward margins of simulated tropical climate zones from the $4\times CO_2$ experiment (Fig. 10b) are matching the reconstructed water masses confined between about 30 °N and 30 °S (Fig. 10a), while in experiments with $8\times CO_2$ or with extensive methane release a significant more poleward 20 °C isotherm is simulated (Fig. 10c and d). The

reconstructed water masses are consistent with the geographical extent of coral reefs (Fig. 13 in Ziegler et al., 2003). Factors controlling coral reefs include temperature, shallow water habitat and available light at the sea floor. Most of the coral reefs are confined to tropical and subtropical waters with temperatures above ~18–20 °C, because the high calcification rates required for vigorous coral growth are limited to warm waters (Fraser and Currie, 1996). In general, coral reefs are also confined to regions of open marine salinities. However, the interpretation of our results serves only as a guide for a change of the general ocean climate pattern, because reconstructed water masses are mostly derived from the sedimentary record of epicontinental seas and coastal regions and because margins of the water masses change constantly with time.

However, uncertainties remain in the modeling studies because of the assumption of too simplified bathymetry. We can speculate that larger deep-sea basins in the Permian may have been ventilated by vertical exchange, internal waves, and turbulent processes. Such exchange processes are not well resolved. Exchange between the deep-sea basins could have taken place by pathways through fracture zones in the mid-ocean ridges, like the modern Romanche Fracture Zone in the equatorial Atlantic. The bathymetric changes may be associated with substantial regional changes in the coupled ocean–atmosphere system (Poulsen et al., 2003).

Another important limitation is that the wind stress and freshwater flux forcing is one-way, i.e. it does not allow for coupled interaction in this study, nor did it in Hotinski et al. (2001), and in Zhang et al. (2001). Because the experimental design allows for forcing LSG with two-dimensional wind stress and freshwater flux from the companion GENESIS 2 Permian simulations (Gibbs et al., 2002), this study gives us important information about thermal feedback for late Paleozoic climate, which is an improvement in comparison to previous studies. Understanding the processes which alter the meridional temperature gradients, magnitude of deep water formation, and strength of the atmospheric and oceanic circulation (e.g. changes of trades and upwelling in the equatorial regions; Otto-Bliesner et al., 2002), will remain a challenging task for fully coupled Permian/Triassic climate simulations with a refined spatial and temporal resolution (J. Kiehl, personal communication; http://www.ccsm.ucar.edu/working_groups/Paleo/reports/040709.html).

Also, the consideration of water-vapor feedback mechanisms may significantly alter the results (Pierrehumbert, 1995; Bates, 1999). Past climate model simulations so far have generally underpredicted polar temperatures (e.g. Barron and Washington, 1982; Gibbs et al., 2002). Clouds coverage may change in response to higher CO_2 via stratospheric circulation and water content (Sloan et al., 1995; Kirk-Davidoff et al., 2002), and this change may contribute to a significant warmer high latitude climate. Also, Permian-to-modern changes in the aerosol loading might be relevant for the radiative budget, but there are no estimates of these properties available so far.

In addition, the solutions of the simulations with the coupled atmospheric energy balance ocean general circulation model could result in multiple steady states (Mikolajewicz and Crowley, 1997). However, we expect that the stability of our simulations is robust because of the asymmetry of the geography of Pangea with respect to the equator.

Another uncertainty arises from the parameterization of mixing by diffusion. The physical processes describing the ventilation of the modern deep-sea are still not well known and controversially discussed (see Pedlosky, 1996; Munk and Wunsch, 1998; Wunsch, 1996). Models are generally tuned to reproduce the modern distribution of water mass properties (temperature and salinity) and tracers, such as radiocarbon or CFCs (e.g. Maier-Reimer et al., 1993). This tuning inevitably depends on the existing topography, again. Thus, the use of different mixing parameterizations could alter the results from the Permian model simulations significantly.

Besides uncertainties associated with the physical approximations several limitations arise from assumptions made for the marine carbon cycle, for example.

Our studies do not consider changes in the marine carbon cycle inventories. For example, Broecker and Peacock (1999) proposed by an analysis of $\delta^{13}C$ for marine carbonates and $\delta^{34}S$ for marine sulfates that with the decline of land plants responsible for the generation of a major portion of the carbon buried, larger amounts were transferred to deep-sea. If so, the deep-sea may have become anoxic by an increased

transfer of organic material from the land surface into the ocean.

Marine sediment geochemistry and potential feedbacks to the atmospheric CO_2 radiative forcing (Archer et al., 1997, 2000b) have not been considered in the studies discussed above. For this reason, we are now undertaking coupled ocean carbon cycle and marine sediment model simulations (Gehlen et al., 2003). Also, the implementation of the sulfur cycle into the model is under development, to allow sulfate reduction for locations of insufficient oxygen concentrations. Recent sediment geochemical models coupled to 3-D ocean carbon models are capable to predict oxic and anoxic diagenesis (e.g. Archer et al., 2002). Such a model provides a more detailed description of sediment processes, which may affect the oxygen concentration above the marine sea floor. For example, a variation in the precipitation of $CaCO_3$ on the seafloor associated with the changes in the thermohaline circulation would affect the pH of the seawater and hence the atmospheric pCO_2 and CO_2 radiative forcing (Archer et al., 2000b). In addition, extra alkalinity is added during bacterial sulfur reduction in an anoxic environment, but this change may only have a second-order impact on the atmospheric pCO_2 (Berner, 2002).

The stoichiometric composition of organic material (Redfield ratio) may have been different during the geologic past so that modern values may be not applicable for the Permian species (see, e.g. Fig. 2.1. in Parrish, 1998, for different ranges in microfossil groups). For example, the marine ecosystem may have been less efficient as a result of the mass extinction (Broecker and Peacock, 1999).

The combined results from this and other Permian dynamic ocean modeling studies indicate that the deep-sea at the Permian–Triassic boundary may have been well ventilated. Large-scale reorganization of the marine carbon cycle, changes in carbon inventories, and a stronger biological pump may be required to explain the anoxic sedimentary deposits.

Acknowledgements

We thank Cornelia Winguth for reading and reviewing this manuscript and David Archer for phanerozoic chemistry discussions. We also thank McAllister Rees and Frederic Fluteau, for helpful reviews which improved the quality of the manuscript. This work was done in collaboration with the Max-Planck-Institut für Meteorology and the Deutsche Forschungsgemeinschaft SPP 1054. Arne Winguth is supported by NASA grant NAG5-11245 and UW Graduate School Research Funds.

Appendix A. Model description

A.1. Coupled energy balance and ocean general circulation model

The coupled atmospheric energy balance model (EBM) (Mikolajewicz, 1996; Mikolajewicz and Crowley, 1997) and the large-scale geostrophic (LSG) ocean general circulation model (Maier-Reimer et al., 1993) are described for the Paleozoic climate simulation in detail in Winguth et al. (2002). The nonlinear EBM is two-dimensional (longitude–latitude), having a single (well-mixed) vertical dimension, a dry atmosphere and the only prognostic quantity is air temperature. The energy budget equation is solved for air temperature with a time step of one day and incorporates incoming solar radiation, outgoing long-wave radiation, and CO_2 radiative forcing. Here we use the functional form of greenhouse gas forcing from Wigley (1987) and a coefficient from Hansen et al. (1988) (consistent with the IPCC 1990 report) to define the changes in the net radiative flux F_{CO2} at the tropopause (in W m^{-2}):

$$F_{CO2} = 6.3\ln\left(pCO_2/\left(pCO_2\right)_{ref}\right) \quad (1)$$

with the preindustrial atmospheric partial pressure $(pCO_2)_{ref}$=280 ppmv.

The incoming solar radiation is either absorbed at the surface, reflected (surface albedo is a function of the ground temperature), or scattered/absorbed by prescribed clouds, ozone, and dust. The solar luminosity is thought to have been steadily increasing since formation, a consequence of conversion of hydrogen to helium. According to calculations by Boothroyd (see Caldeira and Kasting, 1992), we chose for the Permian a reduction of 2.1% relative to the present-day solar constant of 1365 W m^{-2}. Decreases of the Earth's rotation rate from the Permian to present are smaller than 3% and are

neglected in the atmospheric and ocean model simulations. For model simulations discussed below we assumed that the Earth's orbit about the sun was circular (eccentricity = 0) and that the Earth's obliquity (axial tilt) was 23.5°. This setting causes an equal receipt of solar insolation for both hemispheres. A uniform vegetation (mixed tree and grassland or savanna) (Dorman and Sellers, 1989) is imposed at every land grid point of the EBM and is consistent with the formulation of the land surface in the experiments carried out by the GENESIS 2 atmospheric model simulations (Gibbs et al., 2002). This prescribed land surface uniformity is clearly unrealistic; for instance, a significant area of central Pangea was probably desert. However, interpretations of results in comparison with observational evidence would be even more complicated if a non-uniform vegetation is assumed because of vegetation's significant effect on climate (e.g. Dutton and Barron, 1997; DeConto et al., 1999). The horizontal atmospheric transport in the EBM is parameterized as advection by the zonally averaged zonal component of the near-surface wind speed. The heat fluxes between the EBM and ocean model are used to determine the distribution of temperature and sea ice in the mixed layer of the ocean, which is also integrated with a time step of 2 day. The prescribed surface wind speed and freshwater fluxes are computed for the Permian from a GENESIS 2 climate model simulation (Gibbs et al., 2002). The resulting surface conditions serve as the lower boundary conditions for the atmosphere. The atmosphere–ocean heat exchange uses a coupling coefficient κ of 40 W m^{-2} K^{-1} to simulate a strong damping for small-scale temperature changes and is reduced over areas of sea ice coverage. The conductive heat flux through sea ice is inversely proportional to the ice thickness and is proportional to the difference between the air temperature and the sea surface temperature at air temperatures below freezing point. Over land a surface energy balance equation predicts surface temperature with the assumption of zero heat capacity in soil.

The LSG is coupled to the EBM via the surface heat exchange and is also forced by wind stress and freshwater flux (precipitation-minus-evaporation plus river runoff; see Fig. 1 in Winguth et al., 2002) from $4\times CO_2$ and $8\times CO_2$ Wordian simulations of Gibbs et al. (2002), which used the GENESIS 2 climate model (Thompson and Pollard, 1997). In addition, two supplementary experiments, $1\times CO_2$ and $2\times CO_2$, with the same Wordian land configuration in GENESIS 2 have been used to provide additional prescribed values of wind stress, 10 m wind speed, and freshwater fluxes to explore the sensitivity to low atmospheric CO_2 concentrations.

The LSG uses a time step of 15 days, a spatial resolution of $3.5^\circ \times 3.5^\circ$ horizontally and 22 layers vertically, and allows computationally efficient long-term model integrations of several thousand years. The LSG uses two-dimensional fields of heat fluxes, freshwater fluxes, and wind stress (Fig. 1 in Winguth et al., 2002) to predict three-dimensional fields of the ocean currents, potential temperature, salinity, tracers, and two-dimensional fields of sea level, and sea ice thickness. The LSG with 22 vertical layers includes an explicit formulation of vertical diffusion for temperature and salinity (diffusivity ranging from 5×10^{-3} m^2 s^{-1} at the surface to 2×10^{-3} m^2 s^{-1} for the intermediate and deep ocean), which is reduced in the case of very stable vertical stratification by a factor $a/[a+(\delta\rho/\delta z)^2]$ with $a=4\times10^{-7}$ kg^2 m^{-4}. The selection of the diffusion scheme has been tested by various sensitivity experiments to reproduce the observed modern radiocarbon distribution in the ocean (Maier-Reimer et al., 1993; Mikolajewicz, 1996) and the deepening of the mid-to-high latitude thermocline due to winter mixing. Results from these experiments indicated that the mixing of the deep-sea significantly increases with an increase in the diffusion coefficients.

The thermodynamic sea ice model from Maier-Reimer et al. (1993) has been modified to allow not only ocean-driven transport of sea ice due to advection by the mean surface ocean currents predicted by the LSG, but also a wind-driven transport with an assumed equilibrium velocity proportional to the surface wind speed.

A simple river runoff model with a bucket depth of 30 cm is used to transport the net precipitation from the land surface to the coastal ocean areas. The model is initialized for all Wordian experiments with a mean salinity of 34.3 and a mean temperature of about 4 °C (world ocean's average mean temperature today). The reduction in salinity by 0.5 relative to the present-day value is based on the assumption that water stored in

the form of ice, at modern times essentially in Antarctica and Greenland, was probably not present during the Wordian.

A.2. Carbon cycle model

The carbon cycle model applied in this study is similar to the model used in Winguth et al. (1999). The atmospheric CO_2 partial pressure and vertical gradients of carbon are linked with three pumping mechanisms (Volk and Hoffert, 1985): The solubility pump with high solubility at low temperatures, and two biological pumps, the "soft tissue pump" caused by the formation of organic material and depletion of nutrients and carbon in the surface water and the $CaCO_3$ pump. The soft tissue pump can explain about 80% of the vertical gradients of carbon in the ocean. Phosphate, well correlated in most parts of the modern ocean to nitrate, is the nutrient-limiting tracer for photosynthesis, similar to the study of Zhang et al. (2001). Export production, the amount of primary production transported from the euphotic zone into deeper layers is parameterized by the availability of light $I(\phi,t)$, temperature T (in °C), nutrients (PO_4), and vertical mixing v (Maier-Reimer, 1993):

$$EP = c_0 I(\phi,t)(T+2)/(T+10)50m/vPO_4^2 /(P_0+PO_4) \quad (2)$$

with time t, latitude ϕ, $c_0=0.25$, and half saturation constant $P_0=0.02$ μmol L^{-1}. A temperature decrease of 1 °C changes EP by 8% at 5 °C and by 1% at 20 °C.

The models assume a constant Redfield stoichiometry (P:N:C:O_2 ratio) for particulate organic matter (Takahashi et al., 1985). Organic material produced at the surface sinks with a $z^{-0.8}$ declining vertical flux (Martin et al., 1987) into the deep-sea where it is instantaneously remineralized (assuming that the time step of the model is larger than the decomposition of the particulate organic matter). The remineralization of the organic material (POC) is essentially dependent on the available oxygen concentration and on the temperature of the water mass. Remineralization is limited to regions with sufficient oxygen. Unremineralized POC is preserved and advected by the current field. However, one important aspect has not been considered in the recent Permian simulations: Sediment geochemistry is neglected which might be important in particular in areas of high productivity (e.g. the equatorial upwelling regions and the Southern Ocean).

The remineralization of organic debris is simplified in the models which were applied up to now for Paleozoic problems. They treat oxygen as the only oxidant. In regions of anoxia, which are very limited in the modern ocean, several plausible methods have been followed:

1) Oxygen concentrations may take on negative values. This gives an estimate of how much nitrate or sulfate should have been reduced. By this approach, however, regions of low, non-negative values of oxygen are difficult to interpret.
2) Particles may sink through anoxic zones. This approach ignores completely the action of other oxidants and may result in a near bottom accumulation.
3) Particles may be advected as suspended material until they reach oxic zones. In this approach, unrealistically large pools of POC may accumulate, linked to an underestimate of subsurface phosphate maxima. Interpretation of phosphorus and DIC should include the sum of dissolved and particulate species.
4) As sulfur exists in rather high concentrations one can remineralize POC in the absence of oxygen by sulfate reduction.

References

Archer D.E., Kheshgi H., Maier-Reimer E., 1997. Multiple timescales for neutralization of fossil fuel CO2. Geophys. Res., 405–408.

Archer D.E., Eshel G., Winguth A., Broecker W., Pierrehumbert R., Tobis M., Jacob R., 2000a. Atmospheric CO_2 sensitivity to the biological pump in the ocean. Glob. Biogeochem. Cycles 14, 1219–1230.

Archer D.E., Winguth A., Lea D., Mahowald N., 2000b. What causes the glacial/interglacial pCO_2 cycles? Rev. Geophys. 38, 159–189.

Archer D.E., Morford J.L., Emerson S.R., 2002. A model of suboxic sedimentary diagenesis suitable for automatic tuning and gridded global domains. Glob. Biogeochem. Cycles 16.

Barron E.J., Fawcett P.J., 1995. The climate of Pangea: a review of climate model simulations of the Permian. In: Scholle, P.A., Peryt, T.M., Ulmer-Scholle, D.S. (Eds.), The Permian of

Northern Pangea, Paleogeography, Paleoclimates, Stratigraphy, vol. 1. Springer-Verlag, New York, pp. 37–52.
Barron E.J., Washington W.M., 1982. Atmospheric circulation during warm geologic periods: is the equator-to-pole surface-temperature gradient the controlling factor? Geology 10, 633–636.
Bates J.R., 1999. A dynamical stabilizer in the climate system: a mechanism suggested by a simple model. Tellus 51A, 349–372.
Baud A., Magaritz M., Holser W.T., 1989. Permian–Triassic of the Tethys: carbon isotope studies. Geol. Rundsch. 78, 649–677.
Beauchamp B., Baud A., 2002. Growth and demise of Permian biogenic chert along northwest Pangea: evidence for end-Permian collapse of thermohaline circulation. Palaeogeogr. Palaeoclimatol. Palaeoecol. 184, 37–63.
Berger W.H., 1978. Impact of deep sea drilling on paleoceanography. In: Talwani, M., et al., (Eds.), Deep Drilling Results in the Atlantic Ocean: Continental Margins and Paleoenvironment. Am. Geophys Union, Washington, DC, pp. 297–314.
Berner R.A., 1999. Atmospheric oxygen over the Phanerozoic time. Proc. U.S. Natl. Acad. Sci. 96, 10955–10975.
Berner R.A., 2001. Modeling atmospheric O_2 over Phanerozoic time. Geochim. Cosmochim. Acta 65, 685–694.
Berner R.A., 2002. Examination of hypotheses for the Permo–Triassic boundary extinction by carbon cycle modeling. Proc. U.S. Acad. Sci. 99, 4172–4177.
Bice, K.L., 1997. An investigation of early Eocene deep water warmth using uncoupled atmosphere and ocean general circulation models: Model sensitivity to geography, initial temperatures, atmospheric forcing and continental runoff. PhD thesis, University Park, Pennsylvania State University. 363 pp.
Bice K.L., Sloan L.C., Barron E.J., 2000. Comparison of early Eocene isotopic paleotemperatures an the three-dimensional OGCM temperature field: the potential for use of model-derived surface water $\delta^{18}O$. In: Huber, B.T., MacLeod, K.G., Wing, S.C. (Eds.), Warm Climates in Earth History. Cambridge University Press, Cambridge, UK, pp. 79–89.
Bowring S.A., Erwin D.H., Jin Y.G., Martin M.W., Davidek K., Wang W., 1998. U/Pb zircon geochronology and tempo of the end-Permian mass extinction. Science 280, 1039–1045.
Broecker W.S., Peacock S., 1999. An ecologic explanation for the Permo–Triassic carbon and sulfur isotope shifts. Glob. Biogeochem. Cycles 13, 1167–1172.
Caldeira K., Kasting J.F., 1992. The life span of the biosphere revised. Nature 360, 721–723.
Crowley T.J., 2000. Carbon dioxide and Phanerozoic climate. In: Huber, B.T., et al., (Eds.), Warm Climates in Earth History. Cambridge University Press, pp. 425–444.
Crowley T.J., Berner R.A., 2001. Paleoclimate: enhanced: CO2 and climate change. Science 292, 870–872.
DeConto R.M., Hay W.W., Thompson S.L., Bergengren J., 1999. Late Cretaceous climate and vegetation interaction: the cold continental interior paradox. In: Barrera, E., Johnson, C. (Eds.), Evolution of Cretaceaous Oceans/Climate Systems. Geological Society of America Special Paper, vol. 332, pp. 391–406.
Dickens G.R., 2003. Rethinking the global carbon cycle with a large, dynamic and microbially mediated gas hydrate capacitor. Earth Planet. Sci. Lett. (Frontiers) 213, 169–182.
Dorman G.J., Sellers P.J., 1989. A global climatology of albedo, roughness length and stomatal resistance for atmospheric general models as represented by the simple biosphere model (SiB). J. Appl. Meteorol. 28, 833–855.
Dutton J.F., Barron E.J., 1997. Miocene to present vegetation changes, a possible piece of the Cenozoic puzzle. Geology 25, 39–41.
Erwin D.H., 1993. The Great Paleozoic Crisis: Life and Death in the Permian. Columbia Univ. Press, New York. 327 pp.
Erwin D.H., 1994. The Permo–Triassic extinction. Nature 367, 231–236.
Erwin D.H., Bowring S.A., Yugan J., 2002. End-Permian mass extinctions: a review. In: Koerbl, C., MacLeod, K.G. (Eds.), Catastrophic Events and Mass-Extinctions: Impacts and Beyond. Geological Society of America Special Paper, vol. 356, pp. 363–383.
Fluteau F., Besse J., Broutin J., Ramstein G., 2001. The late Permian climate. What can be inferred from climate modelling concerning Pangea scenarios and Hercynian altitude? Palaeogeogr. Palaeoclimatol. Palaeoecol. 167, 39–71.
Fraser R.H., Currie D.J., 1996. The species richness–energy hypothesis in a system where historical factors are thought to prevail: coral reefs. Am. Nat. 148, 138–159.
Gehlen M., Heinze C., Maier-Reimer E., Measures C.I., 2003. Coupled Al–Si geochemistry in an ocean general circulation model: a tool for the validation of oceanic dust deposition fields? Glob. Biogeochem. Cycles 17, 1028.
Gibbs M.T., Rees P.M., Kutzbach J.E., Ziegler A.M., Behling P.J., Rowley D.B., 2002. Simulations of Permian climate and comparisons with climate-sensitive sediments. J. Geol. 110, 33–55.
Hansen J., Fung I., Lacis A., Rind D., Lebedeff S., Ruedy R., Russel G., 1988. Global climate changes as forecast by the GISS's three-dimensional model. J. Geophys. Res. 93, 9341–9364.
Heydari E., Hassanzadeh J., 2003. Deev Jahi model of the Permian–Triassic boundary mass extinction: a case for gas hydrates as the main cause of biological crisis on Earth. Sediment. Geol. 163, 147–163.
Holser W.T., 1977. Catastrophic chemical events in the history of the ocean. Nature 267, 403–408.
Hotinski R.M., Bice K.L., Kump L.R., Najjar R.G., Arthur M.A., 2001. Ocean stagnation and End-Permian anoxia. Geology 29, 7–10.
Hulver M.L., Ziegler A.M., Rowley D.R., Gibbs M.T., 1997. Global latitudinal distribution of Permian to Recent climate-sensitive sediments. Abstr. Programs-Geol. Soc. Am. 29, 6.
Isozaki Y., 1997. Permo–Triassic boundary superanoxia and stratified superocean: records from lost deep sea. Science 276, 235–238.
Kirk-Davidoff B.D., Schrag D.P., Anderson J.G., 2002. On the feedback of stratospheric clouds on polar climate. Geophys. Res. Lett. 29 (11).
Knoll A.H., Bambach R.K., Canfield D.E., Grotzinger J.P., 1996. Comparative earth history and Late Permian mass extinction. Science 273, 452–457.
Krull E.S., Retallack G.J., 2000. ^{13}C depth profiles from paleosols across the Permian–Triassic boundary: evidence for methane release. Geol. Soc. Amer. Bull. 112, 1459–1472.

Kutzbach J.E., Gallimore R.G., 1989. Pangaean climates: megamonsoons of the megacontinent. J. Geophys. Res. 94, 3341–3358.

Kutzbach J.E., Guetter P.J., Washington W.M., 1990. Simulated circulation of an idealized ocean for Pangaean time. Paleoceanography 5, 299–317.

Lenton T.M., 2001. The role of land plants, phosphorus weathering and fire in the rise and regeneration of atmospheric oxygen. Glob. Chang. Biol. 7, 613–629.

Maier-Reimer E., 1993. Geochemical cycles in an ocean general circulation model: preindustrial tracer distributions. Glob. Biogeochem. Cycles 7, 645–677.

Maier-Reimer E., Mikolajewicz U., Hasselmann K., 1993. Mean circulation of the Hamburg LSG OGCM and its sensitivity to the thermohaline surface forcing. J. Phys. Oceanogr. 23, 731–757.

Maier-Reimer E., Mikolajewicz U., Winguth A., 1996. Future ocean uptake of CO2: interaction between ocean circulation and biology. Clim. Dyn. 12, 711–721.

Marotzke J., 1989. Instabilities and multiple steady states of the thermohaline circulation. In: Anderson, D.L.T., Willebrand, J. (Eds.), Oceanic Circulation Models: Combining Data and Dynamics. Kluwer Acad. Press, Norwell, Mass, pp. 501–511.

Martin J.H., Knauer G.A., Karl D., Broenkow W.W., 1987. VERTEX: carbon cycling in the northeast Pacific. Deep-Sea Res., I 34, 267–285.

Mei S., Henderson C.M., 2001. Evolution of Permian conodont provincialism and its significance in global correlation and paleoclimate implication. Palaeogeogr. Palaeoclimatol. Palaeoecol. 170, 237–260.

Mikolajewicz, U., 1996. A meltwater induced collapse of the "conveyor belt" thermohaline circulation and its influence on the distribution of $\Delta^{14}C$ and $\delta^{18}O$ in the oceans. Rep. 189, Max-Planck-Inst. fuer Meteorol., Hamburg, Germany.

Mikolajewicz U., Crowley T.J., 1997. Response of a coupled ocean/energy balance model to restricted flow through the central American isthmus. Paleoceanography 12, 429–441.

Mikolajewicz U., Maier-Reimer E., 1994. Mixed boundary conditions in ocean general circulation models and their influence on the stability of the model's conveyor. J. Geophys. Res. 99 (C11), 22633–22644.

Munk W., Wunsch C., 1998. Abyssal recipes II. Energetics of the tides and wind. Deep-Sea Res. 45, 1976–2009.

Otto-Bliesner B.L., 1993. Tropical mountains and coal formation: a climate model study of the Westphalian (306 Ma). Geophys. Res. Lett. 20, 1947–1950.

Otto-Bliesner B.L., 1998. Effects of tropical mountain elevations on the climate of the Late Carboniferous: climate model simulations. In: Crowley, T.J., Burke, K.C. (Eds.), Tectonic Boundary Conditions for Climate Reconstructions. Oxford University Press, New York, pp. 100–115.

Otto-Bliesner B.L., Brady E.C., Shields C., 2002. Late cretaceous ocean: coupled simulations with the NCAR CSM. J. Geophys. Res.-Atmospheres 107 (D2).

Parrish J.T., 1998. Pre-Quaternary Climate from the Geologic Record. Columbia University Press, New York. 338 pp.

Payne J.L., Lehrmann D.J., Wei J., Orchard M.J., Schrag D.P., Knoll A.H., 2004. Large perturbations of the carbon cycle during recovery from the End-Permian extinction. Science 305, 506–509.

Pedlosky J., 1996. Ocean Circulation Theory. Springer-Verlag, New York. 453 pp.

Pierrehumbert R.T., 1995. Thermostats, radiator fins, and the local runaway Greenhouse. J. Atmos. Sci. 52 (10), 1784–1806.

Poussard P.F., Weaver A.J., Barnes C.R., 1999. Late Ordovician glaciation under high atmospheric CO2: a coupled model analysis. Paleoceanography 14, 542–558.

Poulsen J., Gendaszek S.A., Jacob R.J., 2003. Did the rifting of the Atlantic Ocean cause the Cretaceous thermal maximum? Geology 31, 115–118.

Raup D.M., Sepkoski Jr. J.J., 1982. Mass extinction in the marine fossil record. Science 215, 1501–1503.

Rees P.M., Gibbs M.T., Ziegler A.M., Kutzbach J.E., Behling P.J., 1999. Permian climates: evaluating model predictions using global paleobotanical data. Geology 27, 891–894.

Rees P.M., Ziegler A.M., Gibbs M.T., Kutzbach J.E., Behling P.J., Rowley D.B., 2002. Permian phytogeographic patterns and climate data/model comparisons. J. Geol. 110, 1–31.

Retallack G.J., Smith R.M.H., Ward P.D., 2003. Vertebrate extinction across Permian–Triassic boundary in Karoo Basin, South Africa. GSA Bull. 115, 1133–1152.

Ryskin G., 2003. Methane-driven oceanic eruptions and mass extinctions. Geology 31, 742–744.

Saltzman E.S., Barron E.J., 1982. Deep circulation in the Late Cretaceaous: oxygen isotope paleotemperatures from Inoceramus remains in D.S.D.P. cores. Palaeogeogr. Palaeoclimatol. Palaeoecol. 40, 167–181.

Sarmiento J.L., Herbert T.D., Toggweiler J.R., 1988. Causes of anoxia in the world ocean. Glob. Biogeochem. Cycles 2, 115–128.

Sephton M.A., Looy C.V., Veefkind R.J., Brinkhuis H., De Leeuw J.W., Visscher H., 2002. Synchronous record of $\delta^{13}C$ shifts in the oceans and atmosphere at the end of the Permian. In: Koerbl, C., MacLeod, K.G. (Eds.), Catastrophic Events and Mass-Extinctions: Impacts and Beyond. Geological Society of America Special Paper, vol. 356, pp. 455–462.

Sepkoski Jr. J., 1995. Patterns of Phanerozoic extinction: a perspective from global data bases. In: Walliser, O.H. (Ed.), Global Events and Event Stratigraphy in the Phanerozoic. Springer-Verlag, New-York, pp. 36–51.

Sloan L.C., Walker J.C.G., Moore T.C., 1995. Possible role of oceanic heat transport in early Eocene climate. Paleoceanography 10, 347–356.

Smith, R.S., 2004. Ocean circulation and climate dynamics under idealised continental configurations in a coupled ocean atmosphere model, Southampton University, PhD Thesis. 200 pp.

Strauss H., 1997. The isotopic composition of sedimentary sulfur through time. Paleogeogr., Paleoclimat., Paleoecol. 132, 97–118.

Strauss H., 1999. Geological evolution from isotope proxy signals—sulfur. Chem. Geol. 162, 89–101.

Takahashi T., Broecker W.S., Langer S., 1985. Redfield ratio based on chemical data from isopycnal surfaces. J. Geophys. Res. 90, 6907–6924.

Thompson S.L., Pollard D., 1997. Greenland and Antarctic mass balances for present and doubled atmospheric CO2 from GENESIS version 2 global climate model. J. Climate 10, 871–900.

Twitchett R.J., Loovy C.V., Morante R., Visscher H., Wignall P.B., 2001. Rapid and synchronous collapse of marine and terrestrial ecosystems during the end-Permian biotic crisis. Geology 29, 351–354.

Veizer J., Ala D., Azmy K., Bruckschen P., Buhl D., Bruhn F., Carden G.A.F., Diener A., Ebneth S., Godderis Y., Jasper T., Korte C., Pawellek F., Podlaha O.G., Strauss H., 1999. $^{87}Sr/^{86}Sr$, $\delta^{13}C$ and $\delta^{18}O$ evolution of Phanerozoic sea water. Chem. Geol. 161, 59–88.

Volk T., Hoffert M.I., 1985. Ocean carbon pumps: analysis of relative strengths and efficiencies in ocean-driven atmospheric CO_2 changes. In: Sunquist, E.T., Broecker, W.S. (Eds.), The Carbon Cycle and Atmospheric CO_2: Natural Variations Archean to Present. Geophys. Monogr. Ser., vol. 32. AGU, Washington, D.C., pp. 99–110.

Weidlich O., Kiessling W., Fluegel E., 2003. Permian–Triassic boundary interval as a model for forcing marine ecosystem collapse by long-term atmospheric oxygen drop. Geology 31, 961–964.

Wigley T.M.L., 1987. Relative contributions of different trace gases to the greenhouse effect. Clim. Monit. 16, 14–29.

Wignall P.B., Newton R., 2003. Contrasting deep-water records from the Upper Permian and Lower Triassic of South Tibet and British Columbia: Evidence for a diachronous mass extinction. Palaios 18 (2), 153–167.

Wignall R.J., Twitchett P.B., 2002. Extent, duration, and nature of the Permian–Triassic superanoxic event. In: Koerbl, C., MacLeod, K.G. (Eds.), Catastrophic Events and Mass-Extinctions: Impacts and Beyond. Geological Society of America Special Paper, vol. 356, pp. 383–395.

Winguth A.M.E., Archer D., Maier-Reimer E., Mikolajewicz U., Duplessy J.-C., 1999. Sensitivity of paleonutrient tracer distribution and deep sea circulation to glacial boundary conditions. Paleoceanography 14, 304–323.

Winguth A.M.E., Heinze C., Kutzbach J.E., Maier-Reimer E., Mikolajewicz U., Rowley D.B., Rees P.M., Ziegler A.M., 2002. Simulated warm polar currents during the Middle Permian. Paleoceanography 17 (5), 1057.

Wunsch C., 1996. The Ocean Circulation Inverse Problem. Cambridge University Press. 437 pp.

Zachos J.C., Scott L., Lohmann K.C., 1994. Evolution of early Cenozoic marine temperatures. Paleoceanography 9, 353–387.

Zhang R., Follows M.J., Grotzinger J.P., Marshall J., 2001. Could the Late Permian deep ocean have been anoxic? Paleoceanography 16, 317–329.

Ziegler A.M., Hulver M.L., Lottes A.L., Schmachtenberg W.F., 1984. Uniformitarianism and palaeoclimates: inferences from the distribution of carbonate rocks. In: Brenchley, P.J. (Ed.), Fossils and Climate. John Wiley & Sons, Ltd., Chichester, pp. 3–25.

Ziegler A.M., Hulver M.L., Rowley D.B., 1997. Permian world topography and climate. In: Martini, I.P. (Ed.), Late Glacial and Postglacial Environmental Changes: Quaternary, Carboniferous–Permian, and Proterozoic. Oxford University Press, New York, pp. 111–146.

Ziegler A.M., Gibbs M.T., Hulver M.L., 1998. A mini-atlas of oceanic water masses in the Permian period. Proc. R. Soc. Vic. 110 (1/2), 323–343.

Ziegler A.M., Eshel G., McAllister Rees P., Rothfus T.A., Rowley D.B., Sunderlin D., 2003. Tracing the tropics across land and sea: Permian to present. Lethaia 36, 227–254.